Inorg. Chem. **2005**, *44*, 8628–8641

Biferrocene–$M(mnt)_2$ Charge-Transfer Complexes (M = Ni, Co; mnt = Maleonitriledithiolate). Structure, Valence States, and Magnetic Properties

Tomoyuki Mochida,*,† Kousuke Takazawa,† Hideaki Matsui,† Masashi Takahashi,† Masuo Takeda,† Michiko Sato,‡ Yutaka Nishio,‡ Koji Kajita,‡ and Hatsumi Mori§

Department of Chemistry, Faculty of Science, Toho University, Miyama, Funabashi, Chiba 274-8510, Japan, Department of Physics, Faculty of Science, Toho University, Miyama, Funabashi, Chiba 274-8510, Japan, and Institute for Solid State Physics, The University of Tokyo, Kashiwanoha, Kashiwa-shi, Chiba 277-8581, Japan

Received December 7, 2004

Charge-transfer salts of branched-alkyl biferrocenes, (1′,1‴-R_2-1,1″-biferrocene)[$Ni(mnt)_2$] (**1a**, R = isopropyl; **2a**, R = dineopentyl) and (1′,1‴-R_2-1,1″-biferrocene)$_2$[$Co(mnt)_2$]$_2$ (**1b**, R = isopropyl; **2b**, R = dineopentyl), were prepared. Their valence states were investigated using X-ray crystallography and Mössbauer spectroscopy. Complexes **1a** and **1b** show segregated-stack crystal structures that contain columns of acceptors, whereas structures of **2a** and **2b**, which contain bulky donors, are rather discrete. All of the complexes contain mixed-valent biferrocenium monocations. A two-step valence transition was found in complex **1a**. The crystal contains two crystallographically independent cations: one undergoes valence localization below room temperature; the other undergoes valence localization below ca. 130 K. The former transition is derived from asymmetry of the crystal environment around the cation, whereas the latter one is caused by symmetry lowering coupled with a spin–Peierls transition (T_C = 133.2 K) associated with the dimerization of the acceptors. This compound was found to exhibit a dielectric response based on valence tautomerization. Other complexes (**1b**, **2a**, and **2b**) show a valence-trapped state. In all complexes, charge localization was found to occur through local electrostatic interactions between the donor's cationic moiety and the acceptor's electronegative moieties.

Introduction

Electron transfer in biferrocenium salts in the solid state has attracted considerable attention for years. The electronic states of those salts have been investigated mainly using Mössbauer spectroscopy. Many biferrocenium salts have been synthesized to date, and factors affecting their valence states have been investigated in detail.[1−5] Furthermore, thermal phase isomerization has been discovered in some biferrocenium salts.[5b,c] Therefore, we consider that biferrocenes are intriguing components of functional solids, but most salts synthesized so far contain inorganic anions, such as I_3^-; only a few examples of organic charge-transfer salts have been reported.[6] Under these circumstances, we intend to develop biferrocene-based functional materials for which coexistence and interplay of the electronic systems of the donors and acceptors are expected. To do so, we will introduce organic anions that can carry magnetic spins or

* To whom correspondence should be addressed. E-mail: mochida@chem.sci.toho-u.ac.jp.
† Department of Chemistry, Toho University.
‡ Department of Physics, Toho University.
§ The University of Tokyo.

(1) Hendrickson, D. N. *NATO ASI Ser., Ser. C* **1991**, *343*, 67.
(2) Sano, H. *Hyperfine Interact.* **1990**, *53*, 97.
(3) (a) Webb, R. J.; Dong, T. Y.; Pierpont, C. G.; Boone, S. R.; Chadha, R. K.; Hendrickson, D. N. *J. Am. Chem. Soc.* **1991**, *113*, 4806. (b) Hendrickson, D. N.; Oh, S. M.; Dong, T.-Y.; Kambara, T.; Cohn, M. J.; Moore, M. F. *Comments Inorg. Chem.* **1985**, *4*, 329.
(4) (a) Dong, T.-Y.; Chang, L.-S.; Lee, G.-H.; Peng, S.-M. *Organometallics* **2002**, *21*, 4192. (b) Dong, T.-Y.; Ho, P.-H.; Lai, X.-Q.; Lin, Z.-W.; Lin, K.-J. *Organometallics* **2000**, *19*, 1096 and references cited therein. (c) Dong, T.-Y.; Lee, H.-H.; Chang, C.-K.; Lin, H.-M.; Lin, K.-J. *Organometallics* **1997**, *16*, 2773.
(5) (a) Oda, T.; Nakashima, S.; Okuda, T. *Inorg. Chem.* **2003**, *42*, 5376. (b) Nakashima, S.; Ueki, Y.; Sakai, H.; Maeda, Y. *J. Chem. Soc., Dalton Trans.* **1996**, 139. (c) Nakashima, S.; Oda, T.; Okuda, T.; Watanabe, M. *Inorg. Chem.* **1999**, *38*, 4005.
(6) (a) Nakashima, S.; Iijima, S.; Motoyama, I.; Katada, M.; Sano, H. *Hyperfine Interact.* **1998**, *40*, 315. (b) Iijima, S.; Saida, R.; Motoyama, I.; Sano, H. *Bull. Chem. Soc. Jpn.* **1981**, *54*, 1375. (c) Iijima, S.; Mizutani, F. *Mol. Cryst. Liq. Cryst.* **1998**, *322*, 79. (d) Iijima, S.; Tanaka, Y. *J. Organomet. Chem.* **1984**, *270*, C11.

10.1021/ic048285u CCC: $30.25
Published on Web 10/07/2005

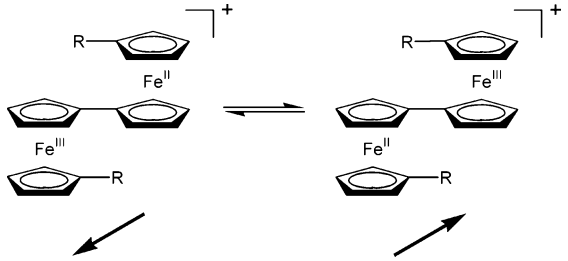

Figure 1. Valence tautomerization coupling with electron transfer in biferrocenium cations. Arrows below the molecules indicate the dipole moment.

conduction electrons. Following this approach, we pursue the possibility of designing molecular magnets accompanying dielectric functions. As a basis of our investigations, we demonstrated previously that the biferrocenium salt exhibits a dielectric response based on polarity inversion mechanism coupling with intramolecular electron transfer (Figure 1).[7] We further elucidated the correlation of structures and physical properties of biferrocene−7,7,8,8-tetracyanoquinodimethane (TCNQ) complexes and discussed the effects of organic anions on mixed-valence states.[8] Along this approach, a novel type of "ionic(I)−ionic(II)" phase transition has been discovered in a biferrocene−F_1TCNQ complex.[9] This paper, which constitutes the fourth part of our investigation, specifically addresses biferrocenium salts of M(mnt)$_2$ anions (mnt = $S_2C_4N_2^{2-}$ = maleonitriledithiolate; M = Ni, Co).

The M(mnt)$_2$ anions are versatile π-conjugated acceptors that are frequently employed as components of molecular conductors and magnets.[10] These acceptors offer several advantages over TCNQ-type acceptors. For example, these molecules exhibit S···S chalcogen−chalcogen interactions in addition to $\pi-\pi$ stacking interactions.[11] Furthermore, particular arrangements of the [Ni(mnt)$_2$]$^-$ monoanion engender ferromagnetic interactions, as demonstrated in ferromagnets (NH$_4$)[Ni(mnt)$_2$]·H$_2$O (T_C = 4.5 K)[12] and other materials.[13−16] The [Ni(mnt)$_2$]$^-$ anion favors one-dimensional columnar molecular arrangements. Paramagnetic−diamagnetic phase transitions involving spin−Peierls-like ones have attracted attention recently.[17] A further advantage is the variation in their molecular stereochemistry and formal

Chart 1. Structural Formulas of **1a**, **1b**, **2a**, and **2b**

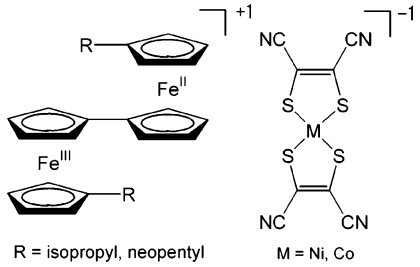

charges: the anions can adopt various electronic states, such as monoanion and dianion (for M = Ni and Co) and a mixed-valent anion [Co(mnt)$_2$]$_3^-$. These have been used as motifs for supramolecular assembly.[18,19] To date, several intriguing M(mnt)$_2$ salts of ferrocene derivatives that exhibit magnetism and electrical conductivity have been synthesized.[20−24] However, no biferrocenium salts with M(mnt)$_2$ anions are known.

1′,1‴-Diisopropyl-1,1″-biferrocene and 1′,1‴-dineopentyl-1,1″-biferrocene were used as donors in this study because these new biferrocenes with branched alkyl chains are designed to produce effective packing in crystals. Conventional dialkylbiferrocenes (R = H, ethyl, *n*-propyl, *n*-butyl) failed to afford single crystals with M(mnt)$_2$. We obtained (1′,1‴-diisopropyl-1,1″-biferrocene)[Ni(mnt)$_2$] (**1a**), (1′,1‴-diisopropyl-1,1″-biferrocene)$_2$[Co(mnt)$_2$]$_2$ (**1b**), (1′,1‴-dineopentyl-1,1″-biferrocene)[Ni(mnt)$_2$] (**2a**), and (1′,1‴-dineopentyl-1,1″-biferrocene)$_2$[Co(mnt)$_2$]$_2$ (**2b**), all of which contain mixed-valent biferrocenium monocations (Chart 1). A preliminary investigation of the structures of **1a** and (1′,1‴-dibenzyl-1,1″-biferrocene)[Ni(mnt)$_2$] has been reported in conference proceedings.[25] We found a two-step valence transition in **1a**, and such a two-step transition seems to be exceptional among the numerous studies of the valence states of biferrocenium salts. We found that a spin−Peierls phase transition originating from the one-dimensional nature of Ni(mnt)$_2$ spins is correlated with this phenomenon. Furthermore, a dielectric response derived from valence tautomerism was demonstrated for this compound. Other complexes, **1b**,

(7) Mochida, T. *Mol. Cryst. Liq. Cryst.* **2000**, *343*, 205.
(8) Mochida, T.; Yamazaki, S.; Suzuki, S.; Shimizu, S.; Mori, H. *Bull. Chem. Soc. Jpn.* **2003**, *76*, 2321.
(9) Mochida, T.; Takazawa, K.; Takahashi, M.; Takeda, M.; Nishio, Y.; Sato, M.; Kajita, K.; Mori, H.; Matsushita, M. M.; Sugawara, T. *J. Phys. Soc. Jpn.* **2005**, *74*, 2214.
(10) Faulmann, C.; Cassoux, P. *Prog. Inorg. Chem.* **2003**, *52*, 399 and references cited therein.
(11) (a) Beswick, C. L.; Schulman, J. M.; Stiefel, E. I. *Prog. Inorg. Chem.* **2003**, *52*, 55 and references cited therein. (b) Alvarez, S.; Vicente, R.; Hoffmann, R. *J. Am. Chem. Soc.* **1985**, *107*, 6253.
(12) Coomber, A. T.; Beljonne, D.; Friend, R. H.; Brédas, J. L.; Charlton, A.; Robertson, N.; Underhill, A. E.; Kurmoo, M.; Day, P. *Nature* **1996**, *380*, 144.
(13) Nishijo, J.; Ogura, E.; Yamaura, J.; Miyazaki, A.; Enoki, T.; Takano, T.; Kuwatani, Y.; Iyoda, M. *Solid State Commun.* **2000**, *116*, 661.
(14) Uruichi, M.; Yakushi, K.; Yamashita, Y.; Qin, J. *J. Mater. Chem.* **1998**, *8*, 141.
(15) Nakajima, H.; Katsuhara, M.; Ashizawa, M.; Kawamoto, T.; Mori, T. *Inorg. Chem.* **2004**, *43*, 6075.
(16) Ren, X.; Chen, Y.; He, C.; Gao, S. *J. Chem. Soc., Dalton Trans.* **2002**, 3915.
(17) (a) Xie, J.; Ren, X.; Song, Y.; Zhang, W.; Liu, W.; He, C.; Meng, Q. *Chem. Commun*. **2002**, 2346. (b) Xie, J.; Ren, X.; He, C.; Song, Y.; Meng, Q.; Kremer, R. K.; Yao, Y. *Chem. Phys. Lett.* **2003**, *369*, 41. (c) Ren, X.; Meng, Q.; Song, Y.; Lu, C.; Hu, C. *Inorg. Chem.* **2002**, *41*, 5686.
(18) Almeida, M.; Henriques, R. T. In *Handbook of Organic Conductive Molecules and Polymers*; Nalwa, H. S., Ed.; John Wiley & Sons: New York, 1997; p 87.
(19) Lewis, G. R.; Dance, I. *J. Chem. Soc., Dalton Trans.* **2000**, 3176.
(20) (a) Zürcher, S.; Petrig, J.; Perseghini, M.; Gramlich, V.; Wörle, M.; Togni, A. *Helv. Chim. Acta* **1999**, *82*, 1324. (b) Zürcher, S.; Gramlich, V.; Arx, D. v.; Togni, A. *Inorg. Chem.* **1998**, *37*, 4015. (c) Hobi, M.; Zürcher, S.; Gramlich, V.; Burckhardt, U.; Mensing, C.; Spahr, M.; Togni, A. *Organometallics* **1996**, *15*, 5342.
(21) Pullen, A. E.; Faulmann, C.; Pokhodnya, I. I.; Cassoux, P.; Tokumoto, M. *Inorg. Chem.* **1998**, *37*, 6714.
(22) (a) Miller, J. S.; Calabrese, J. C.; Epstein, A. J. *Inorg. Chem.* **1989**, *28*, 4230. (b) Fettouhi, M.; Ouahab, L.; Hagiwara, M.; Codjovi, E.; Kahn, O.; Constant-Machado, H.; Varret, F. *Inorg. Chem.* **1995**, *34*, 4152.
(23) Bellamy, D.; Connelly, N. G.; Lewis, R. G.; Orpen, A. G. *CrystEngComm* **2002**, *4*, 51.
(24) Day, M. W.; Qin, J.; Yang, C. *Acta Crystallogr.* **1998**, *C54*, 1413.
(25) Mochida, T.; Matsui, H.; Suzuki, S.; Moriyama, H. *Mol. Cryst. Liq. Cryst.* **2002**, *376*, 295.

Table 1. Crystallographic Parameters for **1a**, **1b**, **2a**, and **2b**

	1a		**1b**		**2a**	**2b**
	$T = 296$ K	$T = 90$ K	$T = 296$ K	$T = 90$ K	$T = 296$ K	$T = 296$ K
empirical formula	$C_{34}H_{30}N_4S_4NiFe_2$	$C_{34}H_{30}N_4S_4NiFe_2$	$C_{34}H_{30}N_4S_4CoFe_2$	$C_{34}H_{30}N_4S_4CoFe_2$	$C_{38}H_{38}N_4S_4NiFe_2$	$C_{38}H_{38}N_4S_4CoFe$
formula weight	793.27	793.27	793.53	793.53	849.38	849.61
crystal system	triclinic	triclinic	triclinic	triclinic	monoclinic	triclinic
space group	$P\bar{1}$ (No. 2)	$P\bar{1}$ (No. 2)	$P1$ (No. 1)	$P1$ (No. 1)	$P2_1/c$ (No. 14)	$P\bar{1}$ (No. 2)
a/Å	13.052(7)	12.86(3)	13.45(4)	13.301(4)	8.409(3)	12.300(4)
b/Å	18.085(8)	17.74(5)	14.31(4)	14.159(4)	23.667(4)	13.212(3)
c/Å	11.542(5)	21.91(6)	19.42(7)	19.387(6)	19.336(4)	12.063(3)
α/deg	91.36(4)	85.97(12)	107.48(5)	106.709(4)	92.66(2)	
β/deg	109.63(4)	76.01(11)	103.40(4)	103.572(2)	94.75(3)	96.93(2)
γ/deg	82.13(5)	81.14(12)	98.18(5)	98.124(3)	100.13(2)	
V/Å^3	2541(2)	4791(22)	3377(18)	3313(2)	3834(1)	1911.1(8)
Z	3	6	4	4	4	2
ρ_{calcd}/(g cm^{-3})	1.555	1.649	1.561	1.591	1.471	1.476
μ/cm^{-1}	16.72	17.73	16.11	16.42	14.82	14.29
diffractometer	Rigaku AFC-5	Rigaku Mercury	Rigaku Mercury	Rigaku Mercury	Rigaku AFC-5	Rigaku AFC-5
refl/param ratio	10.92	14.55	16.51	11.0	11.15	14.23
R_1, R_w[a]	0.046, 0.143	0.055, 0.201	0.050, 0.155	0.034, 0.112	0.049, 0.145	0.037, 0.111
goodness of fit	1.13	0.97	1.00	1.00	1.09	1.01

[a] $R_1 = \Sigma||F_o| - |F_c||/\Sigma|F_o|$, $R_w = [\Sigma w(F_o^2 - F_c^2)^2/\Sigma w(F_o^2)^2]^{1/2}$.

2a, and **2b**, revealed a tendency to exhibit valence-trapped states. As indicated in biferrocenium salts with inorganic anions,[3,4] the symmetry of the crystal environment around the cation was crucial to the valence states also in the present complexes. We present a detailed discussion of the local electrostatic interactions between donors and acceptors, which lead to valence localization.

Experimental Section

Instrumentation. Infrared spectra were recorded on a spectrometer (FT-IR 230; Jasco Inc.) as KBr pellets in the 4000−400 cm^{-1} range. Magnetic susceptibilities were measured using a SQUID susceptometer (MPMS-2; Quantum Design) in the temperature range of 2−300 K at a constant field of 5000 G. The diamagnetic contribution to the magnetic susceptibility of $[Ni(mnt)_2]^-$ was taken from the literature;[14] those of biferrocenes and $[Co(mnt)_2]_2^{2-}$ were calculated using Pascal's law. Intermolecular overlap integrals were calculated based on the extended Hückel molecular orbital method using a software package supplied by Prof. Takehiko Mori (Tokyo Institute of Technology).[26] We measured ^{57}Fe Mössbauer spectra on measuring systems (MDU-1200, DFG-1200, MVT-1000; Wissel GmbH) using ^{57}Co/Rh as the source. Isomer shifts are measured with respect to α-Fe foil at 296 K. Temperature dependence of the dielectric constants of **1a** was measured using an impedance analyzer (Sl 1260; Solartron Analytical) in a frequency range of 1−100 kHz for an alternating electric field of ca. 20 V cm^{-1}. Typical sample dimensions were 1.0 × 0.5 × 0.2 mm^3. Both end surfaces of the plate crystal were painted with silver paste to allow their function as electrodes. Calorimetric measurements of single crystals were carried out using a differential thermal analysis (DTA) method[27] in order that the latent heat and critical behavior of the specific heat in the vicinity of the phase transition are detectable with sufficient accuracy for samples of less than 0.3 mg. Temperatures of the thermal bath and samples were measured using a Cernox resistance thermometer and a chromel−constantan thermocouple with a diameter of 25 μm, respectively. Polystyrene (NIST SRM705a) pellets were used as the reference sample because of the heat capacity[28] similar to those of the samples.

X-ray Structure Analyses. X-ray data were collected using Mo Kα radiation on a Rigaku AFC-5S four-circle diffractometer for **1a** at room temperature (RT), **2a**, and **2b** and a Rigaku Mercury CCD diffractometer for **1a** at 90 K and **1b**. Table 1 lists crystal data, data collection parameters, and analytical statistics. Tables 2 and 3 show selected interatomic distances and angles. All calculations were performed using teXsan[29] or CrystalStructure[30] crystallographic software packages. Structures were solved using direct methods (SIR92[31]) and expanded using Fourier techniques. Nonhydrogen atoms were refined anisotropically. Absorption correction was applied (ψ scan). All hydrogen atoms were inserted at the calculated positions.

Crystallographic data (excluding structure factors) for the structures reported in this paper were deposited with the Cambridge Crystallographic Data Center as supplementary publication nos. CCDC 246263 (**1a** at RT), 246264 (**1a** at 90 K), 246265 (**1b** at RT), 246266 (**1b** at 90 K), 246267 (**2a** at RT), and 246268 (**2b** at RT). Data are available free of charge upon application to CCDC, 12 Union Road, Cambridge CB2 1EZ, U.K. [fax (+44)1223-336-033; e-mail deposit@ccdc.cam.ac.uk].

Preparation of 1′,1‴-Diisopropyl-1,1″-biferrocene. (a) 1-Bromo-1′-(2-hydroxyisopropyl)ferrocene. A solution of 1,1′-dibromoferrocene (8.67 g, 24.5 mmol) in tetrahydrofuran (20 mL) was cooled to −25 °C under a dinitrogen atmosphere. To this solution was added *n*-butyllithium in hexane (14.5 mL, 22.2 mmol) dropwise over 30 min. The solution was stirred for 1 h at −25 °C, and acetone (1.5 mL, 20.4 mmol) was added in one portion. After stirring for 1 h more, the solution was allowed to warm to room temperature and then extracted with ether. The organic layer was washed three times with water and then dried over magnesium sulfate. The solvent was removed by evaporation; the resultant oily material was purified using column chromatography (silica gel; eluent, dichloromethane). 1-Bromo-1′-(2-hydroxyisopropyl)ferrocene was obtained as a brown oil (yield 38.8%).

(26) Mori, T.; Kobayashi, A.; Sasaki, Y.; Kobayashi, H.; Saito, G.; Inokuchi, H. *Bull. Chem. Soc. Jpn.* **1984**, *57*, 627.
(27) Schilling, A.; Jeandupeux, O. *Phys. Rev. B* **1995**, *52*, 9714.
(28) Chang, S. S.; Bestul, A. B. *J. Polym. Sci., Polym. Phys. Ed.* **1968**, *6*, 849.
(29) *teXsan: Crystal Structure Analysis Package*; Molecular Structure Corp.: The Woodlands, TX, 1999.
(30) *CrystalStructure, Single-Crystal Structure Analysis Software*, Version 3.1; Molecular Structure Corp.: The Woodlands, TX, and Rigaku Corp.: Akishima, Tokyo, Japan, 2002.
(31) Altomare, A.; Cascarano, G.; Giacovazzo, C.; Guagliardi, A.; Burla, M. C.; Polidori, G.; Camalli, M. *J. Appl. Crystallogr.* **1994**, *27*, 435.

Table 2. Selected Intramolecular Distances (Å) for **1a**, **1b**, **2a**, and **2b**

			1a (296 K)				
Fe(1)−C(Cp1[a])	2.048(5)−2.116(5)	(avg 2.075)	Fe(1)−C(Cp2[b])	2.041(6)−2.125(4)	(avg 2.070)		
Fe(2)−C(Cp1)	2.042(6)−2.099(5)	(avg 2.060)	Fe(2)−C(Cp2)	2.023(6)−2.087(4)	(avg 2.054)		
Fe(3)−C(Cp1)	2.043(5)−2.106(5)	(avg 2.068)	Fe(3)−C(Cp2)	2.040(6)−2.103(5)	(avg 2.065)		
Fe(1)−Cp1[c]	1.695(3)	Fe(3)−Cp1	1.684(3)	Fe(2)−Cp1	1.682(3)	Fe(3)−Cp2	1.675(3)
Fe(1)−Cp2[c]	1.683(3)			Fe(2)−Cp2	1.665(3)		
			1a (90 K)				
Fe(1)−C(Cp1)	2.047(6)−2.126(6)	(avg 2.075)	Fe(1)−C(Cp2)	2.046(6)−2.124(6)	(avg 2.073)		
Fe(2)−C(Cp1)	2.035(5)−2.073(6)	(avg 2.050)	Fe(2)−C(Cp2)	2.034(6)−2.048(6)	(avg 2.041)		
Fe(3)−C(Cp1)	2.036(5)−2.071(6)	(avg 2.050)	Fe(3)−C(Cp2)	2.037(6)−2.047(6)	(avg 2.042)		
Fe(4)−C(Cp1)	2.044(5)−2.128(6)	(avg 2.078)	Fe(4)−C(Cp2)	2.045(6)−2.120(6)	(avg 2.072)		
Fe(5)−C(Cp1)	2.040(5)−2.096(5)	(avg 2.060)	Fe(5)−C(Cp2)	2.036(5)−2.082(6)	(avg 2.053)		
Fe(6)−C(Cp1)	2.042(5)−2.099(5)	(avg 2.059)	Fe(6)−C(Cp2)	2.030(5)−2.090(6)	(avg 2.055)		
Fe(1)−Cp1	1.690(5)	Fe(4)−Cp1	1.691(5)	Fe(1)−Cp2	1.684(5)	Fe(4)−Cp2	1.684(5)
Fe(2)−Cp1	1.657(5)	Fe(5)−Cp1	1.668(5)	Fe(2)−Cp2	1.645(5)	Fe(5)−Cp2	1.658(5)
Fe(3)−Cp1	1.657(5)	Fe(6)−Cp1	1.673(5)	Fe(3)−Cp2	1.646(5)	Fe(6)−Cp2	1.661(5)
			1b (296 K)				
Fe(1)−C(Cp1)	2.014(1)−2.071(1)	(avg 2.042)	Fe(1)−C(Cp2)	2.010(1)−2.040(1)	(avg 2.024)		
Fe(2)−C(Cp1)	2.020(1)−2.115(1)	(avg 2.061)	Fe(2)−C(Cp2)	2.042(1)−2.129(1)	(avg 2.074)		
Fe(3)−C(Cp1)	2.012(2)−2.063(1)	(avg 2.027)	Fe(3)−C(Cp2)	1.970(1)−2.041(1)	(avg 2.017)		
Fe(4)−C(Cp1)	2.047(1)−2.090(1)	(avg 2.063)	Fe(4)−C(Cp2)	2.052(1)−2.111(1)	(avg 2.072)		
Fe(5)−C(Cp1)	2.006(1)−2.052(1)	(avg 2.035)	Fe(5)−C(Cp2)	2.002(1)−2.053(1)	(avg 2.020)		
Fe(6)−C(Cp1)	2.007(1)−2.077(1)	(avg 2.040)	Fe(6)−C(Cp2)	2.022(1)−2.125(1)	(avg 2.065)		
Fe(7)−C(Cp1)	2.023(1)−2.042(1)	(avg 2.031)	Fe(7)−C(Cp2)	2.015(1)−2.052(1)	(avg 2.032)		
Fe(8)−C(Cp1)	2.037(1)−2.083(1)	(avg 2.060)	Fe(8)−C(Cp2)	2.045(1)−2.112(1)	(avg 2.065)		
Fe(1)−Cp1	1.665(7)	Fe(5)−Cp1	1.652(8)	Fe(1)−Cp2	1.635(7)	Fe(5)−Cp2	1.630(7)
Fe(2)−Cp1	1.683(7)	Fe(6)−Cp1	1.663(8)	Fe(2)−Cp2	1.692(7)	Fe(6)−Cp2	1.685(7)
Fe(3)−Cp1	1.654(8)	Fe(7)−Cp1	1.653(8)	Fe(3)−Cp2	1.629(8)	Fe(7)−Cp2	1.639(7)
Fe(4)−Cp1	1.690(8)	Fe(8)−Cp1	1.679(7)	Fe(4)−Cp2	1.693(8)	Fe(8)−Cp2	1.681(7)
			1b (90 K)				
Fe(1)−C(Cp1)	2.036(2)−2.071(3)	(avg 2.048)	Fe(1)−C(Cp2)	2.042(2)−2.066(3)	(avg 2.050)		
Fe(2)−C(Cp1)	2.049(3)−2.133(3)	(avg 2.092)	Fe(2)−C(Cp2)	2.060(3)−2.149(2)	(avg 2.092)		
Fe(3)−C(Cp1)	2.028(4)−2.065(3)	(avg 2.049)	Fe(3)−C(Cp2)	2.028(3)−2.059(3)	(avg 2.046)		
Fe(4)−C(Cp1)	2.078(3)−2.114(3)	(avg 2.090)	Fe(4)−C(Cp2)	2.066(3)−2.103(3)	(avg 2.082)		
Fe(5)−C(Cp1)	2.033(5)−2.063(4)	(avg 2.046)	Fe(5)−C(Cp2)	2.035(3)−2.056(3)	(avg 2.047)		
Fe(6)−C(Cp1)	2.044(7)−2.121(4)	(avg 2.080)	Fe(6)−C(Cp2)	2.042(3)−2.123(3)	(avg 2.070)		
Fe(7)−C(Cp1)	2.033(3)−2.058(4)	(avg 2.046)	Fe(7)−C(Cp2)	2.037(3)−2.065(3)	(avg 2.048)		
Fe(8)−C(Cp1)	2.064(3)−2.118(3)	(avg 2.095)	Fe(8)−C(Cp2)	2.059(3)−2.133(3)	(avg 2.095)		
Fe(1)−Cp1	1.654(2)	Fe(5)−Cp1	1.645(2)	Fe(1)−Cp2	1.653(2)	Fe(5)−Cp2	1.647(2)
Fe(2)−Cp1	1.706(2)	Fe(6)−Cp1	1.696(2)	Fe(2)−Cp2	1.705(2)	Fe(6)−Cp2	1.677(2)
Fe(3)−Cp1	1.651(2)	Fe(7)−Cp1	1.652(2)	Fe(3)−Cp2	1.650(2)	Fe(7)−Cp2	1.646(2)
Fe(4)−Cp1	1.706(2)	Fe(8)−Cp1	1.710(2)	Fe(4)−Cp2	1.694(2)	Fe(8)−Cp2	1.694(2)
			2a (296 K)				
Fe(1)−C(Cp1)	2.032(6)−2.079(5)	(avg 2.054)	Fe(1)−C(Cp2)	2.047(6)−2.070(6)	(avg 2.055)		
Fe(2)−C(Cp1)	2.069(6)−2.117(6)	(avg 2.082)	Fe(2)−C(Cp2)	2.058(6)−2.112(5)	(avg 2.076)		
Fe(1)−Cp1	1.663(3)	Fe(2)−Cp1	1.697(3)	Fe(1)−Cp2	1.665(3)	Fe(2)−Cp2	1.691(3)
			2b (296 K)				
Fe(1)−C(Cp1)	2.041(4)−2.060(4)	(avg 2.054)	Fe(1)−C(Cp2)	2.031(4)−2.063(4)	(avg 2.049)		
Fe(2)−C(Cp1)	2.059(3)−2.118(3)	(avg 2.080)	Fe(2)−C(Cp2)	2.054(4)−2.126(3)	(avg 2.085)		
Fe(1)−Cp1	1.662(2)	Fe(2)−Cp1	1.697(2)	Fe(1)−Cp2	1.656(2)	Fe(2)−Cp2	1.699(2)

[a] Cp1: Cp ring with alkyl groups. [b] Cp2: Cp ring in the fulvalenide moiety. [c] Distance between Fe and centroid of Cp.

Table 3. Tilt Angles (deg) between the Two Cp Rings in the Fulvalenide Moieties for **1a**, **1b**, **2a**, and **2b**

1a	296 K	Cp2(Fe1)−Cp2(Fe2)	4.6(4)	Cp2(Fe3)−Cp2(Fe3)	0
	90 K	Cp2(Fe1)−Cp2(Fe2)	4.6(2)	Cp2(Fe3)−Cp2(Fe4)	3.9(2)
		Cp2(Fe5)−Cp2(Fe6)	1.7(2)		
1b	296 K	Cp2(Fe1)−Cp2(Fe2)	5.7(4)	Cp2(Fe3)−Cp2(Fe4)	3.6(6)
		Cp2(Fe5)−Cp2(Fe6)	6.1(4)	Cp2(Fe7)−Cp2(Fe8)	6.9(4)
	90 K	Cp2(Fe1)−Cp2(Fe2)	10.6(2)	Cp2(Fe3)−Cp2(Fe4)	2.8(2)
		Cp2(Fe5)−Cp2(Fe6)	7.5(2)	Cp2(Fe7)−Cp2(Fe8)	9.9(2)
2a	296 K	Cp2(Fe1)−Cp2(Fe2)	3.7(4)		
2b	296 K	Cp2(Fe1)−Cp2(Fe2)	3.6(2)		

(b) 1-Bromo-1′-isopropylferrocene. To a solution of 1-bromo-1′-(2-hydroxyisopropyl)ferrocene (3.07 g, 9.51 mmol) in diethyl ether (30 mL) was added lithium aluminum hydride (1.08 g, 28.5 mmol) in small portions under a dinitrogen atomosphere. After stirring for a few minutes, aluminum chloride (3.80 g, 28.5 mmol) was added in small portions, and the resulting solution was stirred overnight. The solution was cooled in an ice bath; then small amounts of methanol and water were added. The reaction mixture was extracted with ether, washed twice with water, and dried over magnesium sulfate. The solvent was removed by evaporation. The crude product was purified using a short plug of alumina (eluent, hexane). 1-Bromo-1′-isopropylferrocene was obtained as a brown oil (yield 68.5%).

(c) 1′,1‴-Diisopropyl-1,1-biferrocene. A mixture of 1-bromo-1′-isopropylferrocene (2.00 g, 6.51 mmol) and activated copper (4.14 g, 65.1 mmol) was heated at 125 °C under a dinitrogen

atmosphere for 26 h. After cooling, the solid was extracted with dichloromethane and filtered through a Celite plug. The solvent was removed by evaporation and purified using column chromatography (alumina; eluent, hexane). The product was purified by recrystallization from dichloromethane/hexane to yield orange crystals of 1′,1‴-diisopropyl-1,1″-biferrocene (yield 20.8%). ^{1}H NMR ($CDCl_3$, ppm): 1.10 (d, 12H), 2.48 (m, 2H), 3.84 (t, 4H), 3.87 (t, 4H), 4.13 (t, 4H), 4.29 (t, 4H).

Preparation of (1′,1‴-Diisopropyl-1,1″-biferrocene)[Ni(mnt)$_2$] (1a). To a solution of 1′,1‴-diisopropyl-1,1″-biferrocene (26 mg, 5.7×10^{-2} mmol) in dichloromethane (2 mL) was added a solution of ferrocenium bis(maleonitriledithiolato)nickel(III)[19c] (30 mg, 5.7×10^{-2} mmol) in dichloromethane/acetone [1:2 (v/v), 3 mL]. Single crystals of **1a** were obtained through vapor diffusion of pentane into the solution at room temperature under a dinitrogen atmosphere: 27 mg of black plates (yield 59%). IR (KBr, cm^{-1}): 2962, 2208, 1641, 1526, 1476, 1448, 1416, 1388, 1365, 1305, 1159, 1107, 1034, 997, 919, 818, 675, 606, 501, 418. Anal. Calcd for $C_{34}H_{30}N_4S_4Fe_2Ni$: C, 51.48; H, 3.81; N, 7.06. Found: C, 51.25; H, 3.85; N, 7.07.

Preparation of (1′,1‴-Diisopropyl-1,1″-biferrocene)$_2$[Co(mnt)$_2$]$_2$ (1b). To a solution of 1′,1‴-diisopropyl-1,1″-biferrocene (3 mg, 6.6×10^{-3} mmol) in dichloromethane (0.5 mL) was added a solution of ferrocenium hexafluorophosphate (2.2 mg, 6.6×10^{-3} mmol) in acetone (0.5 mL) through a filter plug. After stirring for a few minutes, a hot acetonitrile solution (2 mL) of (NBu_4)[Co(mnt)$_2$][32] (3.4 mg, 6.6×10^{-3} mmol) was added dropwise, and the resulting solution was stirred for a few minutes. Single crystals of **1b** were obtained by slow evaporation of the solution at room temperature: 1.7 mg of black prismatic crystals (yield 32%). It was difficult to obtain pure materials in larger scales because of the deposition of other components upon recrystallization. IR (KBr, cm^{-1}): 3101, 2927, 2218, 2202, 1525, 1473, 1446, 1417, 1386, 1363,1309, 1207, 1159, 1145, 1111, 1070, 1053, 1033, 1022, 1001, 918, 848, 817. Anal. Calcd for $C_{34}H_{30}N_4S_4Fe_2Co$: C, 51.46; H, 3.81; N, 7.06. Found: C, 50.79; H, 4.03; N, 7.39.

Preparation of 1′,1‴-Dineopentyl-1,1″-biferrocene. (a) 1-Bromo-1′-(1-hydroxyneopentyl)ferrocene. 1,1′-Dibromoferrocene (5.63 g, 15.9 mmol) was placed in a freshly dried three-necked flask (100 mL) and then dried under vacuum. Dried tetrahydrofuran (50 mL) followed by *n*-butyllithium (10.0 mL, 1.59 M in hexane) was added under dinitrogen. The resulting solution was stirred at −25 °C for 1 h, during which time 1-lithio-1′-bromoferrocene gradually precipitated. Pivalaldehyde (1.73 mL, 15.9 mmol) was then added. The solution was stirred further at −25 °C for another 1.5 h. After quenching with water, the resulting mixture was extracted with ether. The combined extracts were dried over magnesium sulfate and evaporated under reduced pressure. The residue was chromatographed on a column of neutral alumina. Elution with CH_2Cl_2/hexane (1:4) gave eluates that yielded the desired compound (3.40 g, 41.9%).

(b) 1-Bromo-1′-neopentylferrocene. An excess of aluminum chloride was added in small portions to a mixture of 1-bromo-1′-(1-hydroxyneopenthyl)ferrocene (3.40 g, 9.41 mmol) in dry ether (60 mL) under dinitrogen. An excess of lithium aluminum hydride was added to this solution. Then the mixture was stirred at room temperature for 12 h. After quenching with water, the resulting mixture was extracted with ether. The combined extracts were dried over magnesium sulfate and evaporated at reduced pressure. The residue was chromatographed on a column of alumina. Elution with hexane gave eluates that yielded the desired compound (2.28 g, 70.3%).

(c) 1′,1‴-Dineopentyl-1,1′-biferrocene. 1-Bromo-1′-neopentylferrocene (2.28 g, 6.61 mmol) was mixed thoroughly with activated copper (0.42 g). That mixture was heated at 135 °C (oil bath) for 22 h. The solid was cooled to room temperature and extracted with CH_2Cl_2. The combined extracts were dried over magnesium sulfate and evaporated under reduced pressure. The residue was chromatographed on a column of alumina. Elution with hexane gave elutes that yielded 1′,1‴-dineopentyl-1,1″-biferrocene (1.05 g, 62.2%). ^{1}H NMR ($CDCl_3$, ppm): 4.22 (t, 4H), 4.09 (t, 4H), 3.86 (t, 4H), 3.80 (t, 4H), 2.02 (s, 4H), 0.73 (s, 18H).

Preparation of (1′,1‴-Dineopentyl-1,1″-biferrocene)[Ni(mnt)$_2$] (2a). This material was prepared as described for **1a** using 1′,1‴-dineopentyl-1,1″-biferroceneferrocenium (30 mg, 5.9×10^{-2} mmol) and bis(maleonitriledithiolato)nickel(III) (31 mg, 5.9×10^{-2} mmol): 37 mg of black prismatic crystals (yield 73%). IR (KBr, cm^{-1}): 3099, 2947, 2864, 2208, 1636, 1559, 1524, 1474, 1464, 1438, 1387, 1362, 1318, 1282, 1235, 1159, 1109, 1036, 998, 896, 836, 818, 754, 735, 684, 602, 569, 501, 450, 418. Anal. Calcd for $C_{38}H_{38}N_4S_4Fe_2Ni$: C, 53.73; H, 4.51; N, 6.60. Found: C, 53.49; H, 4.45; N, 6.85.

Preparation of (1′,1‴-Dineopentyl-1,1″-biferrocene)$_2$[Co(mnt)$_2$]$_2$ (2b). This material was prepared as described for **1b** using 1′,1‴-dineopentyl-1,1″-biferrocene (30 mg, 5.6×10^{-2} mmol) in dichloromethane (3 mL), ferrocenium hexafluorophosphate (20 mg, 5.6×10^{-2} mmol) in acetone (3 mL), and (NBu_4)[Co(mnt)$_2$] (34 mg, 5.6×10^{-2} mmol) in acetonitrile (3 mL): 34 mg of black prismatic crystals (yield 69%). IR (KBr, cm^{-1}): 3101, 2960, 2929, 2906, 2862, 2202, 1527, 1473, 1465, 1452, 1392, 1365, 1282, 1232, 1157, 1109, 1064, 1043, 1002, 921, 894. Anal. Calcd for $C_{38}H_{38}N_4S_4Fe_2Co$: C, 53.71; H, 4.51; N, 6.60. Found: C, 53.56; H, 4.59; N, 6.57.

Results and Discussion

Preparation and General Structural Features. 1′,1‴-Diisopropyl and 1′,1‴-dineopentyl derivatives of biferrocenes were prepared by applying standard procedures.[33] M(mnt)$_2$ salts of these biferrocenes were synthesized by metathesis using biferrocenium cations generated in situ and M(mnt)$_2$ anions. All salts contained mixed-valent monocations of donors. The Ni(mnt)$_2$ salts (**1a** and **2a**) exhibit 1:1 D/A stoichiometry, with their formula being represented as (Donor)[Ni(mnt)$_2$]. The intramolecular geometry of the anion was virtually identical with that in (N^nBu$_4$)[Ni(mnt)$_2$];[34] it was confirmed to be a monoanion also from the infrared −CN stretching vibration observed at 2208 cm^{-1}.[35] In Co(mnt)$_2$ salts (**1b** and **2b**), pairs of Co(mnt)$_2$ anions combine to form discrete centrosymmetric dimers [Co(mnt)$_2$]$_2^{2-}$, with intramolecular Co···Co distances of ca. 3.12 Å. The formulas of these salts are thus described as (Donor)$_2$[Co(mnt)$_2$]$_2$. The intramolecular geometry of the anion was virtually identical with that in (N^nBu$_4$)$_2$[Co(mnt)$_2$]$_2$.[36] The [Co(mnt)$_2$]$_2$ unit was confirmed to be a dianion also by the infrared −CN

(32) Holm, R. H.; Davison, A. *Inorg. Synth*. **1967**, *10*, 8.

(33) (a) Lai, L. L.; Dong, T.-Y. *Synthesis* **1995**, 1231. (b) Dong, T.-Y.; Lai, L. L. *J. Organomet. Chem.* **1996**, *509*, 131.

(34) Mochida, T.; Suzuki, S.; Moriyama, H.; Terao, H.; Sugawara, T. *Acta Crystallogr*. **2000**, *C56*, 1183.

(35) Best, S. P.; Ciniawsky, S. A.; Clark, R. J. H.; McQueen, R. C. S. *J. Chem. Soc., Dalton Trans*. **1993**, 2267.

(36) Mochida, T.; Takazawa, K.; Matsushita, M. M.; Sugawara, T. *Acta Crystallogr*. **2002**, *C58*, m431.

stretching vibration observed at 2202 cm^{-1}. We further prepared a Pt(mnt)$_2$ salt of 1′,1‴-diisopropyl-1,1″-biferrocene, which was isomorphous to **1a**.[37] However, further characterization was not performed because of extremely low yield.

Regarding the general packing structures of the complexes, we found that segregated-stack structures are formed in **1a** and **1b**, whereas discrete structures are formed in **2a** and **2b**. Although the arrangement of the anions in **2a** was somewhat columnar, the intermolecular overlap within the column is small because of slipped molecular arrangements. These structural features suggest that the donor with the bulkier neopentyl substituent prevents the formation of columnar structures of the acceptors and engenders packing structures that are less symmetrical. The neopentyl donor exhibited virtually the same molecular structures in both **2a** and **2b**, whereas the isopropyl donor exhibited flexible conformations in **1a** and **1b**. Concerning the acceptors, comparison of **1a**−**2a** and **1b**−**2b** shows that [Co(mnt)$_2$]$_2$, which is less planar than Ni(mnt)$_2$, affords structures that are more complicated. Being consistent with these structural features, all of the complexes were insulators in terms of electrical conductivity. As we have demonstrated in a previous study,[8] the valence states in biferrocenium salts with organic acceptors are largely affected by cation−anion electrostatic interactions and by the packing environments around the cations. In the valence-localized structures of the present complexes, the formal charge in the biferrocenium cations was found to adhere on either of the two ferrocenyl moieties of the donor such that it has stronger interaction with the electronegative moieties of the acceptors. This observation suggests that electrostatic interactions are the principal cause of valence localization. The following sections describe the structures and electronic states of individual complexes and present discussions of intermolecular interactions on their valence states.

Structure and Valence States of 1a. Complex **1a** was found to exhibit an unusual two-step valence transition. In the following sections, we will present detailed experimental results and discuss its origin; the crystal contains two crystallographically independent biferrocenium cations, one of which undergoes valence localization at around room temperature, whereas the other one undergoes below ca. 130 K coupling with a spin−Peierls transition of the acceptor. By focusing on local structures, we show that both valence orderings result from local asymmetry of the crystal environment around the cations.

(a) Crystal Structure at Room Temperature. The packing diagram of **1a** at room temperature is shown in Figure 2a. The complex crystallizes in the centrosymmetric space group $P\bar{1}$ and exhibits a segregated-stack structure. Two crystallographically independent acceptor molecules exist, anions a and b. The former molecule is located on the inversion center. The acceptor molecules are stacked along the *c* axis in an almost regular fashion; they show $\pi-\pi$-stacking interactions within the column. The shortest Ni···Ni and Ni···S distances between anions a and b are 3.8444(7) and 3.614(2) Å, respectively. The shortest Ni···Ni and Ni···S distances between two anions b are 3.863(1) and 3.731(2) Å, respectively. Thus, the degree of trimerization (b···a···b) is only slight. The overlap integrals between the acceptors were calculated using the Hückel molecular orbital approximation. The intratrimer and intertrimer overlap integrals are 9.5×10^{-3} and 11.9×10^{-3}, respectively. Thus, the intratrimer interaction is slightly stronger than the intertrimer interaction, but they are comparable.

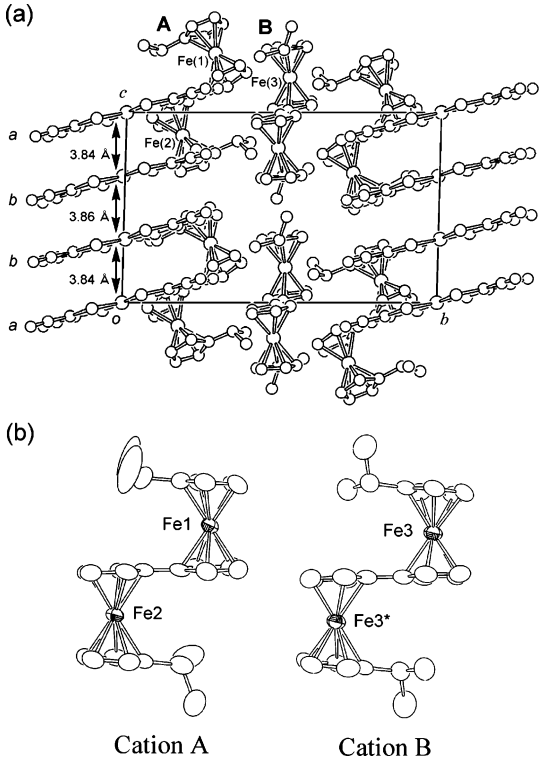

Figure 2. (a) Crystal structure of **1a** at room temperature viewed along the *a* axis. The Ni···Ni intermolecular distances between the acceptors are also shown. (b) ORTEP drawings of the molecular structures of **1a** with the numbering scheme. Displacement ellipsoids are shown at the 50% probability level. Hydrogen atoms are omitted for clarity. Numbering schemes for the donors in **2a** and **2b** are the same as that for cation A.

Figure 2b shows the ORTEP[38] drawings of the cations. The unit cell contains two crystallographically independent biferrocenium cations, denoted as cations A and B. The intramolecular Fe···Fe distances are 5.16−5.17 Å. The crystal contains two kinds of independent columns that are formed by $\pi-\pi$ stacking of the donors: one is formed by cation A, which runs parallel to the acceptor column; the other is formed by cation B, located between the cation A columns and acceptors. Cation B resides on the center of

(37) (1′,1‴-Dineopentyl-1,1″-biferrocene)[Pt(mnt)$_2$]: This material was prepared as described for **1a** using a ferrocenium salt of [Pt(mnt)$_2$] and 1′,1‴-dineopentyl-1,1′-biferrocene. Yield: black needles. IR (KBr, cm^{-1}): 3434, 3096, 2954, 2857, 2210, 1636, 1526, 1465, 1436, 1388, 1363, 1235, 1162, 1109, 1036, 838, 819, 679, 603. The starting materials are often recovered, and we could rarely isolate the product. Crystallographic parameters at 296 K: monoclinic, $P2_1/c$ (No. 14), $a = 8.471(3)$ Å, $b = 23.627(2)$ Å, $c = 19.254(2)$ Å, $\beta = 93.49(2)°$, $V = 3846(1)$, and $Z = 4$. The cell volume of the complex was slightly larger (by 0.3%) than that of **1a**, reflecting the larger atomic radii of the Pt atom.

(38) ORTEP-3 for Windows: Farrugia, L. J. *J. Appl. Crystallogr.* **1997**, *30*, 565.

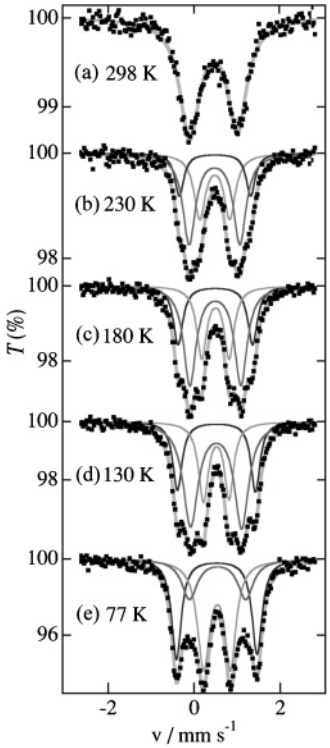

Figure 3. Temperature dependence of the ^{57}Fe Mössbauer spectra of **1a**, recorded at (a) 298 K, (b) 230 K, (c) 180 K, (d) 130 K, and (e) 77 K. Fitting lines with the parameters listed in Table 4 are also shown.

symmetry and involves two crystallographically equivalent Fe atoms. The average Fe(3)−C(Cp) distance is 2.066 Å, which is between the values for a neutral ferrocene (2.05 Å) and a ferrocenium cation (2.08 Å),[39] indicating the occurrence of valence tautomerization. The Fe−C(Cp) distances are generally used as measures for the valence states of ferrocenes, but there is often a dispersion of the individual bond lengths. On the other hand, cation A shows a slightly asymmetric molecular structure. The average Fe(1)−C(Cp) distance in the ferrocene unit involving Fe(1) is 2.077 Å, whereas the corresponding value for the other ferrocene unit involving Fe(2) is 2.056 Å. These values indicate that the former unit is closer to a ferrocenium cation, whereas the latter unit is closer to a neutral ferrocene. The Fe−Cp(centroid) distances, which are also used to estimate the valence state of ferrocenes, are consistent with the tendency found from the Fe−C distances. Furthermore, the 1′- and 1‴-alkyl substituents have slightly different conformations (Figure 2b, left). Although the structure indicates a somewhat localized tendency of the valence state of cation A, Mössbauer spectra indicated that a rapid exchange occurs at room temperature and that valence localization becomes noticeable with further lowering of the temperature.

(b) Mössbauer Spectra. We measured ^{57}Fe Mössbauer spectra to elucidate characteristics of the valence states in **1a** and found an unusual temperature dependence. The spectra and least-squares fitting parameters are shown in Figure 3 and Table 4, respectively. At room temperature, the spectrum consists of a pair of quadrupole doublets (Figure 3a), which indicates rapid valence exchange between Fe(II) and Fe(III). A localized component appears with decreasing temperature, and coexistence of the trapped and averaged components is visible (Figure 3b). Interestingly, the spectra remain almost unchanged down to ca. 130 K (Figure 3c,d). With further decreases of temperatures below 130 K, the spectrum exhibits two pairs of quadrupole doublets (Figure 3e), indicating complete valence localization. The unusual temperature dependence can be explained by successive valence transitions of the two crystallographically independent molecules at different temperatures: with decreasing temperature below room temperature, cation A undergoes gradual valence localization caused by the asymmetric crystal environment, whereas cation B, sitting on the center of symmetry, continues to undergo tautomerization. With further decreasing temperature, cation B undergoes valence localization at temperatures below 130 K. This interpretation was further supported by structure determination at low temperature.

Table 4. ^{57}Fe Mössbauer Least-Squares Fitting Parameters for **1a**, **2a**, and **2b**

compound	T/K	δ^a/(mm s^{-1})	$\Delta E_Q{}^b$	$\Gamma_1{}^c$/(mm s^{-1})	$\Gamma_2{}^c$/(mm s^{-1})
1a	298	0.45	1.11	0.56	0.54
	230	0.47	1.18	0.35	0.35
		0.49	1.66	0.25	0.25
		0.48	0.70	0.32	0.32
	180	0.49	1.19	0.35	0.35
		0.49	1.73	0.27	0.27
		0.50	0.64	0.28	0.28
	130	0.52	1.19	0.42	0.40
		0.52	1.82	0.26	0.25
		0.51	0.60	0.28	0.26
	77	0.54	1.31	0.44	0.44
		0.53	1.88	0.27	0.28
		0.53	0.62	0.35	0.31
2a	298	0.44	1.74	0.25	0.22
		0.43	0.53	0.26	0.28
	77	0.52	1.98	0.25	0.25
		0.53	0.42	0.37	0.37
2b	298	0.46	2.14	0.29	0.28
		0.43	0.38	0.40	0.32

[a] Isomer shift referenced to iron foil at room temperature. [b] Quadrupole split. [c] Full width at half-height taken from the least-squares fitting program.

(c) Crystal Structure at 90 K. The structure of **1a** was determined at low temperature to obtain structural information on the valence transition. The unit cell at 150 K was almost identical with that at room temperature. However, a marked change of structure was observed at 90 K, as shown in the packing diagram in Figure 4.[40] We observed three important changes at that temperature: (i) cell doubling along the *c* axis, (ii) strong dimerization of the acceptors, and (iii) removal of the inversion center from cation B. These indicate that the valence transition below ca. 130 K is associated with a phase transition that is accompanied by symmetry lowering of the crystal lattice, although the centrosymmetric space group ($P\bar{1}$) is maintained. Consistently, calorimetric measurement revealed the presence of a phase transition at T_C = 133.2 K (vide infra). The geometries of independent anions

(39) Geib, S. J.; Rheingold, A. L.; Dong, T.-Y.; Hendrickson, D. N. *J. Organomet. Chem.* **1986**, *312*, 241.

(40) The low-temperature unit cell has been taken such that the new *c* axis is along the $2c_{RT} + a_{RT}$ direction, from a crystallographical standpoint. Thus, the columnar structure is extending along the $-a + c$ direction in the low-temperature unit cell.

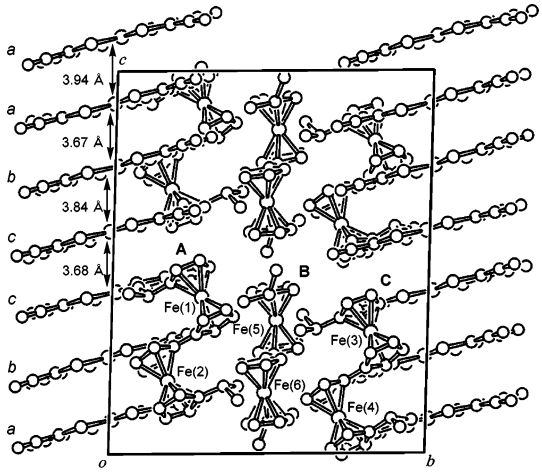

Figure 4. Packing diagram of **1a** at 90 K viewed along the *a* axis. The Ni···Ni intermolecular distances between the acceptors are also shown.

are the same within experimental errors, and no such thing as charge separation is suggested.

The Ni···Ni distances between the Ni(mnt)$_2$ anions are shown in Figure 4. Anions a−b and anions c−c form dimers, with their respective Ni···Ni distances being 3.68(1) and 3.67(1) Å. In contrast, the interdimer distance for anions a−a and that for b−c become longer: the respective Ni···Ni distances are 3.94(1) and 3.84(1) Å. The overlap integrals between the acceptors were calculated to estimate the variation of intermolecular interactions within the column. The intradimer and interdimer overlap integrals are 19.6×10^{-3} (for a−b) and 21.2×10^{-3} (for c−c), whereas the interdimer integrals are 4.2×10^{-3} (for a−a) and 5.0×10^{-3} (for b−c), which indicates that the degree of dimerization is fairly strong.

Next, we focus on the local structures of the biferrocenium cations. At 90 K, cation A has a fully valence-trapped structure: the Fc(1) unit is in the form of a ferrocenium cation [Fe(1)−C(Cp) = 2.074 Å] and the Fc(2) unit is neutral [Fe(2)−C(Cp) = 2.046 Å]. These values indicate a stronger tendency of valence localization than those found at room temperature, in accordance with results of Mössbauer spectroscopy. The situation for cation C, containing Fe(3) and Fe(4), is very similar. The following observation suggests that the valence localization can be reasonably understood in terms of local cation−anion electrostatic interactions. We specifically address the local environments around the donors. Shown in Figure 5a is the local environment around cation A at room temperature. Intermolecular distances between the iron atoms and the anions that are shorter than 5 Å are indicated in the figure. Above and below the cations are located the Cp rings of the adjacent donors, whereas the right and left sides of the Fe atoms are surrounded by anions. Fc(1) is surrounded by two cyano groups of the acceptors [Fe(1)···NC−: 4.06 and 4.41 Å], whereas Fc(2) is surrounded by one cyano group [Fe(2)···NC−: 4.26 Å] and a sulfur atom [Fe(2)···S: 4.53 Å] of the acceptors. The shorter donor−acceptor contacts for Fc(1) indicate that the unit interacts more strongly with the anions. Corresponding distances at 90 K are also shown in the figure in parentheses.

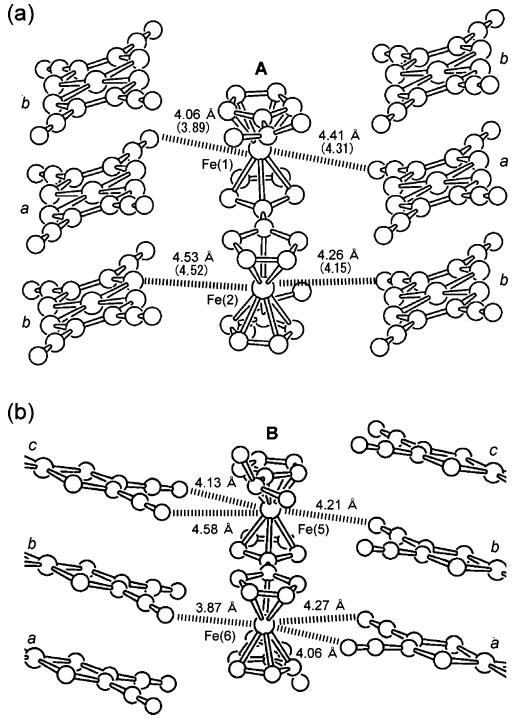

Figure 5. (a) Local environment around cation A in **1a** at room temperature. Short distances (<5 Å) between the iron atoms and the anions are also shown together with those at 90 K in parentheses. Dashed lines are merely guides to the eye. (b) Local environment around cation B in **1a** at 90 K.

On the other hand, regarding cation B, the center of symmetry on this molecule, which existed in the room temperature phase, has been removed. In this phase, the molecular structure becomes crystallographically asymmetric. The average Fe−C(Cp) bond lengths of cation B are almost identical for Fe(5) and Fe(6), with the latter being only slightly closer to a ferrocenium cation. Therefore, the valence state for this cation seems to remain somewhat average at this temperature; structure determination at lower temperature would reveal a fully valence-trapped structure. In this phase, the environment around the cations becomes asymmetric, and the resultant asymmetric cation−anion interaction probably causes valence localization. At room temperature, both Fe centers are in the same environment, surrounded by two CN groups of anion a [−CN···Fe(3): 4.29 and 4.61 Å] and a CN group of anion b [−CN···Fe(3): 4.25 Å]. However, Figure 5b shows that the environment around the two ferrocene units becomes different at 90 K: the corresponding distances for Fe(5) become 4.13, 4.58, and 4.21 Å, whereas those for Fe(6) become 3.87, 4.27, and 4.06 Å. Therefore, the shorter distances for the latter cause stronger cation−anion interactions, inducing charge localization on Fe(6). Judging from this situation, the valence localization of cation B below ca. 130 K can be regarded as a result of the dimerization of the anions, which causes symmetry lowering of the environment around the cation, i.e., the asymmetric cation−anion interactions.

(d) Specific Heat. Calorimetric studies of single crystals were carried out by adopting a DTA method to elucidate the thermodynamic character of the phase transition in **1a**. Figure 6a shows the molar heat capacity in the process of

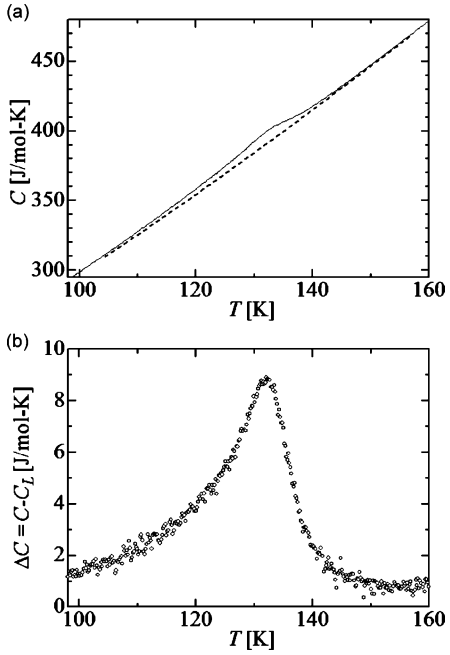

Figure 6. (a) Temperature dependence of the specific heat of **1a**. The dashed line shows the lattice contribution C_L estimated from the polynomial fitting. (b) Excess heat capacity $\Delta C = C - C_L$ around the spin−Peierls transition temperature.

heating at a scan rate of 32 mK s^{-1}. A small peak was found at around 133 K, corresponding to the phase transition, with no hysteresis in heating and cooling processes within the resolution limit. The dashed line in Figure 6a shows the lattice contribution for the heat capacity as estimated by polynomial fitting. Figure 6b depicts the excess heat capacity obtained by subtracting the estimated lattice contribution. The transition temperature was determined to be $T_C = 133.2$ K; reversibility of this excess term indicated the second-order nature of the phase transition. The resulting excess entropy estimated by integration of the excess term is 0.4 J mol^{-1} K^{-1}. The maximum value ($\Delta C_{Max} > 8$ J mol^{-1} K^{-1}) of the excess heat capacity is several times larger than that expected by BCS mean-field theory. Furthermore, the temperature dependence of the excess contribution does not show the mean-field-type jump but exhibits a sharp peak. These features are attributable to the effect of fluctuation, which is enhanced in a quasi-one-dimensional system in the critical temperature region.[44,45]

The second-order nature of the transition, along with the dimerization of one-dimensional $Ni(mnt)_2$ spins as shown above, indicates unambiguously that the phase transition is a spin−Peierls type.[41] The small excess entropy (0.4 J mol^{-1} K^{-1}) can be explained by strong antiferromagnetic interactions between the acceptor spins above T_C, and this small value is further evidence that the valence ordering in the biferrocenium cations is an indirect result of the spin−Peierls transition and not the cause of the phase transition; if the transition is of an order−disorder type, the entropy change would be $R \ln 2 = 5.7$ J mol^{-1}. The valence localization itself is not a cooperative transition but a thermal depopulation process under the asymmetrical crystal environment resulting from the dimerization of the acceptors. This interpretation also presents a reasonable explanation for gradual valence trapping below the phase transition temperature. In comparison to conventional spin−Peierls systems,[41,42] the high transition temperature ($T_C = 133.2$ K) is noteworthy. In some $Ni(mnt)_2$ salts, paramagnetic−diamagnetic phase transitions associated with dimerization were found with transition temperatures that range up to ca. 180 K,[17] but most of these transitions seem to have some external origin other than a pure spin−Peierls transition, in contrast to the present case, as manifested in their first-order nature.

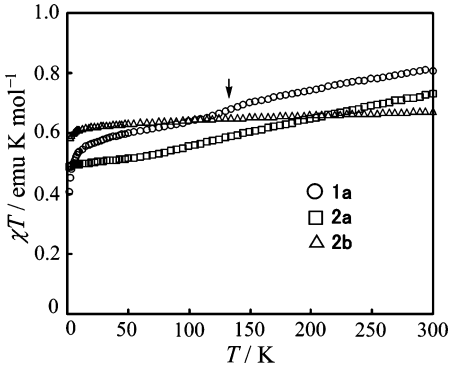

Figure 7. Temperature dependence of the magnetic susceptibilities of **1a**, **2a**, and **2b**, represented in the form of χT vs T. The small arrow indicates the spin−Peierls transition temperature for **1a**, where the decrease of susceptibilities is observable.

Considering the origin of the valence localization processes, the two-step valence transition is the consequence of introducing the open-shell anion that is subject to spin−Peierls instability. The isomorphous $Pt(mnt)_2$ salt may exhibit slightly different transition properties because large spin−orbit interactions exist in $Pt(mnt)_2$.[13]

(e) Magnetic Susceptibility. Details of the magnetic properties of all of the complexes will be given later, but for convenience, the result for **1a** is briefly described here. The magnetic susceptibility of complex **1a** is shown in Figure 7 (open circles) in the form of χT vs T plots, which decrease monotonically with decreasing temperature. We could observe the spin−Peierls transition in **1a** as a slight decrease of χT at around 130 K, as indicated by an arrow in the figure. Dimerization of the acceptors at the spin−Peierls transition usually accompanies a prominent decrease of the magnetic susceptibility,[41,42] but in the present case, the transition appeared as a small decrease in χT. This is because the magnetic susceptibility is dominated by the contribution of the ferrocenium spins having larger magnetic moments; further-

(41) Musfeldt, J. L. In *Magnetism: Molecules to Materials, Models and Experiments*; Miller, J. S., Drillon, M., Eds.; Wiley-VCH: Weinheim, Germany, 2001; Chapter 3.
(42) (a) Huizinga, S.; Kommandeur, J.; Sawatzky, G. A.; Thole, B. T. *Phys. Rev. B* **1979**, *19*, 4723. (b) Oseroff, S. B.; Cheong, S.-W.; Aktas, B.; Hundley, M. F.; Fisk, Z.; Rupp, L. W., Jr. *Phys. Rev. Lett.* **1995**, *74*, 1450. (c) Bray, J. W.; Hart, H. R., Jr.; Interrante, L. V.; Jacobs, I. S.; Kasper, J. S.; Watkins, G. D.; Wee, S. H.; Bonner, J. C. *Phys. Rev. Lett.* **1975**, *35*, 745. (d) Mukai, K.; Wada, N.; Jamali, J. B.; Achiwa, N.; Narumi, Y.; Kindo, K.; Kobayashi, T.; Amaya, K. *Chem. Phys. Lett.* **1996**, *257*, 538.
(43) Klokishner, S.; Boukheddaden, K.; Varret, F. *Phys. Rev. B* **1999**, *60*, 150.
(44) Ma, S. K. *Modern Theory of Critical Phenomena*; Benjamin: New York, 1976.
(45) A detailed discussion will be published elsewhere.

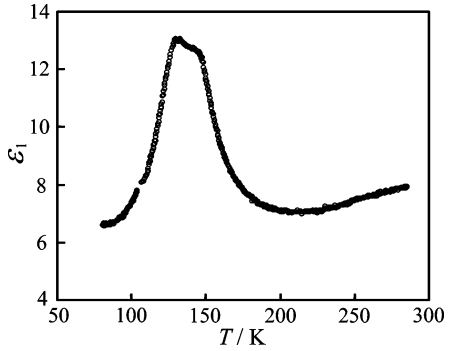

Figure 8. Temperature dependence of the real part of the dielectric constants of **1a** measured at 100 kHz.

more, contribution from the acceptor spins above T_C becomes smaller because of strong antiferromagnetic interactions ($J/k_B = -207.2$ K, vide infra). Accordingly, the magnetic gap below the transition temperature could not be determined.

(f) Dielectric Constants. We further investigated the dielectric response of **1a** because the electron transfer in the biferrocenium cation is accompanied by a polarity inversion, as depicted in Figure 1.[7] Figure 8 shows the temperature dependence of the dielectric constants of **1a** measured at 100 kHz. The dielectric constant decreases slightly with decreasing temperature down to 200 K. Concomitant with decreasing temperature, a remarkable dielectric enhancement is observed: it exhibits a maximum at 133 K, at which temperature the phase transition occurs. The response was reversible against temperature. That enhancement, with no frequency dependence, is reasonably attributable to the rapid valence tautomerization of cation B in the crystal, with the decrease below 133 K corresponding to valence ordering. Essential features of the dielectric response are in close agreement with those we reported previously for biferrocenium triiodides,[7] but it is noteworthy that dipole−dipole interaction is not the driving force for the valence ordering here. In inorganic biferrocenium salts, dipole−dipole interactions between the donors can cause antiferroelectric valence-ordering phase transitions,[3,43] but these types of interactions are less effective here because of the presence of the large anions. Valence localization in **1a** occurs in an antiferroelectric fashion as observed at 90 K, but this is merely because of the centrosymmetric space group. A slight frequency dependence was observed at temperatures greater than 200 K. It may originate either from the relaxation processes of tautomerization of cation A or from the contribution of electrical conduction along the Ni(mnt)$_2$ columns.

Structure and Valence States of 1b. Structure determination for this complex was carried out at room temperature and at 90 K. No remarkable differences were found. Therefore, we focus this discussion on the low-temperature structure, which was determined more precisely. Packing diagrams of **1b** at 90 K are shown in Figure 9a,b. For simplicity, only the molecules on the (100) plane are shown in Figure 9a, whereas only those on the (200) plane are shown in Figure 9b. The complex crystallizes in the noncentrosymmetric space group $P1$ and forms a segregated-stack structure. Although the structure is similar to that of **1a**, it is much

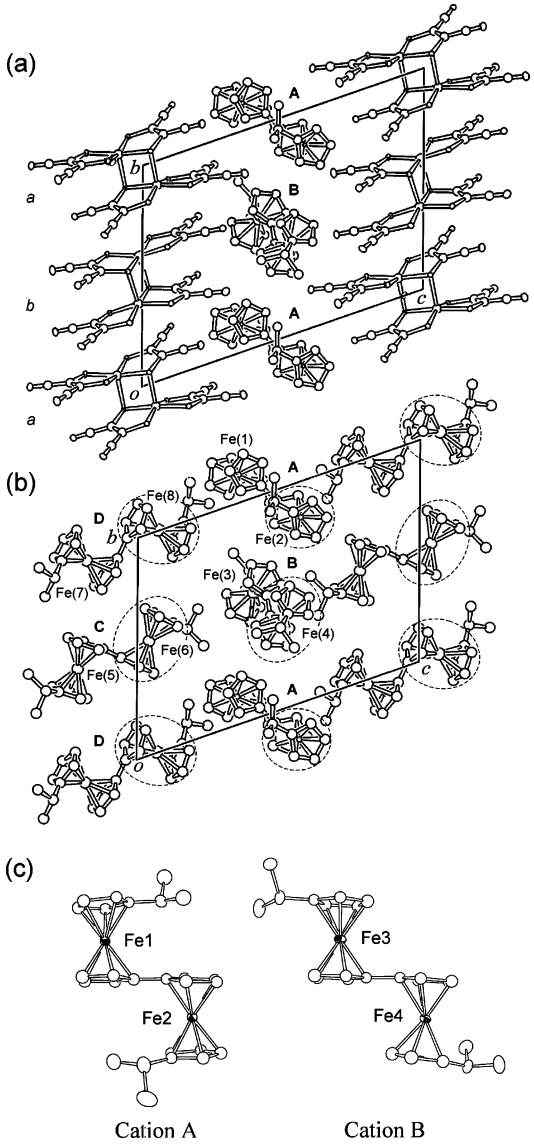

Figure 9. Packing diagrams of **1b** viewed along the *a* axis, showing (a) molecules on the (100) planes and (b) molecules on the (200) planes. Dashed circles represent the ferrocenium units. (c) ORTEP drawings of the molecular structures of cations A and B in **1b** at 90 K with the numbering scheme. Displacement ellipsoids are shown at the 80% probability level. Hydrogen atoms are omitted for clarity.

more complicated. The crystal has four crystallographically independent biferrocenium cations (cations A−D) and two $[Co(mnt)_2]_2^{2-}$ dimers (anions a and b). The ORTEP diagrams of cations A and B are shown in Figure 9c. These molecules adopt syn and anti conformations, respectively, with respect to the positions of the substituents. Cations C and D also exhibit anti conformation, but the conformations of the alkyl groups differ slightly from each other.

The $[Co(mnt)_2]_2^{2-}$ dimers are arranged along the *b* axis, in which anions a and b are stacked alternately in a parallel fashion (Figure 9a). The geometries of these anions are similar, but the deviation from planarity is larger in anion a. Interdimer interactions are very small; S···S distances of 3.67−3.70 Å are present between the dimers, but these are slightly longer than the contact distances. The interdimer Co···S and Co···Co distances are 3.99 and 4.83−4.90 Å, respectively.

The donor forms two kinds of columns along the *b* axis in the crystal (Figure 9b). The column formed by cations C and D runs adjacent to the acceptor column, whereas the other column formed by cations A and B is located between the columns of cations C and D and those of the acceptors. The presence of two kinds of columns is also observed in **1a** as well as in (1′,1‴-dibenzoyl-1,1″-biferrocene)[Ni(mnt)$_2$].[25] However, the present complex is unique in that the molecules are stacked in a canted arrangement, exhibiting no $\pi\cdots\pi$-stacking interactions.

Examination of the bond lengths of the cation at 90 K revealed that this complex has a valence-trapped structure. All independent donor molecules have asymmetric structures in which one Fc site is in a cationic form [Fe(n)−C(Cp) = 2.08−2.10 Å, for n = 2, 4, 6, and 8] and the other site is in a neutral form [Fe(n)−C(Cp) = 2.04−2.06 Å, for n = 1, 3, 5, and 7]. The ferrocenium moieties are represented as dashed circles in Figure 9b. Here we discuss the local environments around the donors to account for valence localization in terms of local cation−anion electrostatic interactions. Concerning cations C and D, which constitute parallel columns sandwiched between the anion columns, the Fc(6) and Fc(8) units are located just between the anions and effectively interact with the anions, whereas Fc(5) and Fc(7) are slipped outside the anion columns and have less electrostatic interaction. Therefore, stronger electrostatic interactions for the former units can stabilize the cationic charge residing on them. Concerning cation B, Fe(4) is surrounded by five cyano groups of acceptors (−CN$\cdots$Fe distances: 4.4−5.1 Å) and Fe(3) by two cyano groups (−CN$\cdots$Fe distances: 4.1−5.1 Å). This situation can cause charge localization on the former unit. Furthermore, the ferrocenium moiety of cation B is faced with the neutral moiety of cation A and the neutral ferrocene moiety of cation B with the ferrocenyl moiety of cation A, and vice versa, which seems to be an additional factor favoring valence localization. This kind of interaction, which avoids energetically unfavorable cation−cation contacts, may become more important in the case of cation A because both Fc units of this cation are surrounded by five cyano groups (−CN$\cdots$Fe distances: 4.3−5.2 Å) and have similar cation−anion interactions. As described above, the extent of interactions that induces valence localization is different for the four independent cations. Therefore, the molecules may have different valence detrapping temperatures, if any. Considering the crystallographic asymmetry and the strength of the local electrostatic interactions described above, the valence states of cations C and D are likely to remain trapped at elevated temperatures, whereas those in cation A may become averaged more easily. However, judging from the intramolecular geometry, the valence states of the biferrocenium cations seem to remain localized at room temperature. Temperature-dependent Mössbauer spectroscopy is necessary for detailed examination of the valence states, but it was unavailable because of the difficulty in collecting a sufficient quantity of samples.

Structures and Valence States of 2a and 2b. The packing diagram of **2a** is shown in Figure 10a. The complex crystallizes in the space group $P2_1/c$. Figure 10b shows a columnar arrangement of the anions, which extends along the *a* axis. Within the column, the molecules are arranged in slipped configurations such that intermolecular interaction exists at the molecule edges. The intermolecular Ni$\cdots$Ni distances are 4.828(2) and 5.003(2) Å. The intermolecular S$\cdots$S distances of 3.701(3) and 3.777(3) Å, which are slightly longer than the contact distances, indicate that there are no direct S$\cdots$S interactions. Two kinds of interactions occur between the acceptors, as denoted by S_1 and S_2 in Figure 10b. Although the interaction modes seem to differ significantly, the overlap integrals were found to be nearly identical: S_1 and S_2 are 11.3×10^{-3} and 11.4×10^{-3}, respectively. These values are comparable to those in **1a** at room temperature. The lowest unoccupied molecular orbital of Ni(mnt)$_2$ has a nodal plane on the metal atom and the overlap integrals are susceptible to molecular orientation. The overlap integrals in **1a** become small despite the face-to-face arrangement because of molecular canting within the column.

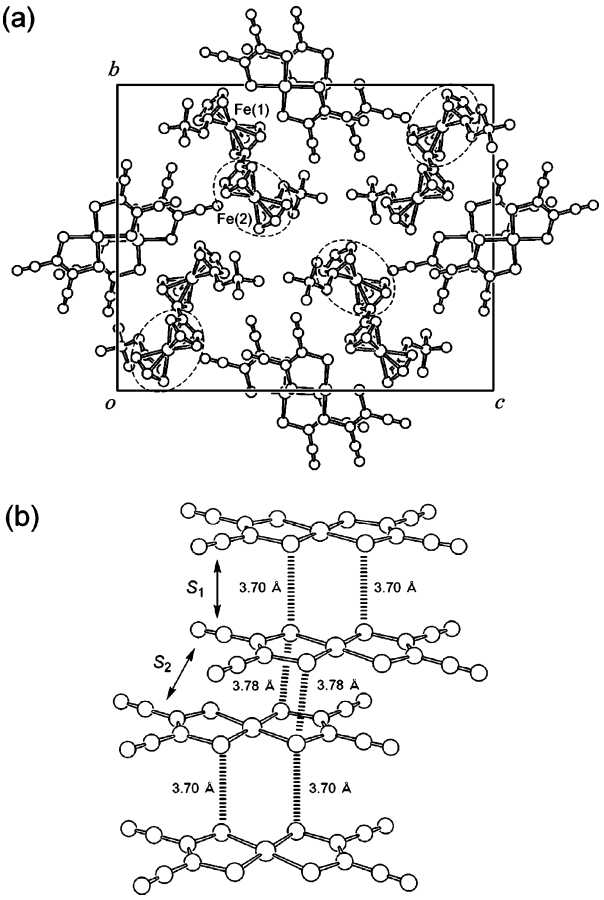

Figure 10. (a) Packing diagram of **2a** viewed along the *a* axis. Dashed circles represent the ferrocenium units. (b) Arrangement of Ni(mnt)$_2$ anions in **2a** in its columnar structure. Dotted lines are merely guides to the eye. S_1 and S_2 indicate the definitions of overlap integrals (see the text).

The biferrocene molecule in **2a** has a valence-trapped state. Figure 11a shows the ^{57}Fe Mössbauer spectrum of this complex recorded at room temperature, which displays two pairs of quadrupole doublets, being typical of the valence-trapped state.[4−6] The result is consistent with the crystal structure; the average Fe(1)−C(Cp) distances in the ferrocene units involving Fe(1) and Fe(2) are 2.055 and 2.079 Å,

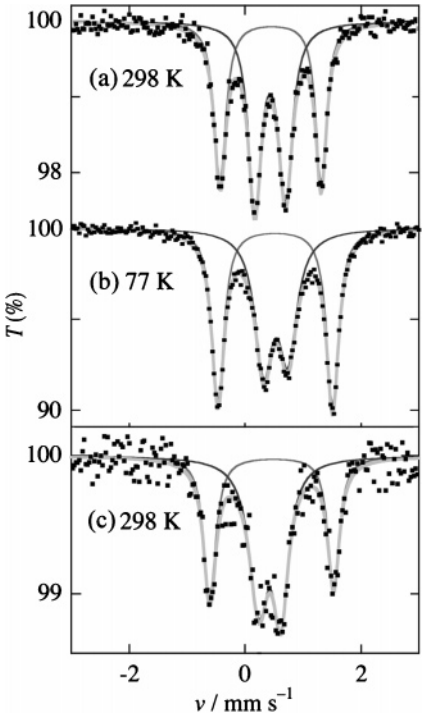

Figure 11. ^{57}Fe Mössbauer spectra of (a) **2a** at 298 K, (b) **2a** at 77 K, and (c) **2b** at 298 K. Fitting lines with the parameters listed in Table 4 are also shown.

respectively. These values indicate that Fc(1) corresponds to a neutral ferrocene whereas Fc(2) corresponds to a ferrocenium unit. The ferrocenium units are indicated by dashed circles in Figure 10a. The intramolecular Fe···Fe distance is 5.12 Å. As seen in parts a and b of Figure 11, splitting between the outer and inner doublets becomes greater with decreasing temperature, indicating that charge localization becomes complete at low temperatures. The fitting parameters for the spectra are shown in Table 4.

Complex **2b** also exhibits a valence-trapped state. The ^{57}Fe Mössbauer spectrum of **2b** at 295 K is shown in Figure 11c, in which two pairs of doublets are observed. This spectrum indicates localization of the valence states, in agreement with the molecular geometries determined by X-ray crystallography. The packing diagram of **2b** is shown in Figure 12. The $[Co(mnt)_2]_2^{2-}$ dimers are located at the origins of the lattice to form a discrete structure with no significant interdimer interactions. The interdimer Co···Co distance is 9.46 Å. The biferrocenium cation has an asymmetric structure, with the average Fe(1)−C(Cp) distance of 2.051 Å and the Fe(2)−C(Cp) distance of 2.083 Å. These values indicate that Fc(1) and Fc(2) correspond respectively to a neutral ferrocene and a ferrocenium cation. The cationic moieties are indicated by dashed circles in Figure 12. The intramolecular distance between Fe···Fe atoms is 5.14 Å. The Mössbauer spectrum of **2b** (Figure 11c) shows that valence localization is complete at room temperature. It is noteworthy that the degree of splitting in the spectrum of **2b** at room temperature is almost identical with that of **2a** at 77 K, which indicates that **2b** has a stronger valence-trapping tendency than **2a**. The least-squares fitting parameters of these spectra are listed in Table 4.

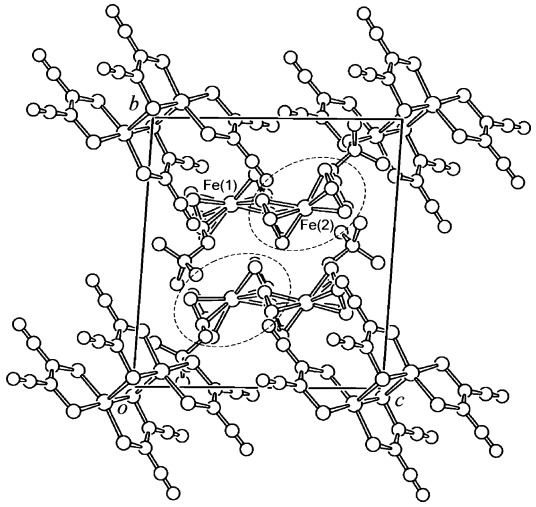

Figure 12. Packing diagram of **2b** viewed along the *a* axis. Dashed circles represent ferrocenium units.

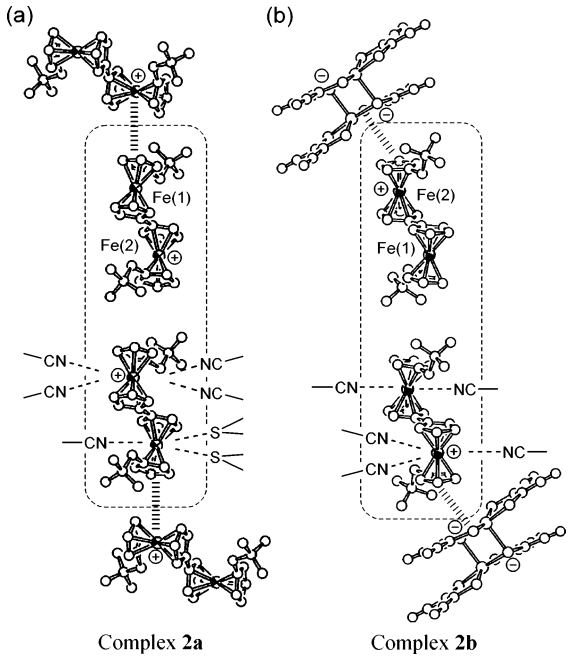

Figure 13. Local environment around the centrosymmetric dimer units of donors in (a) **2a** and (b) **2b**. Dashed lines indicate cation−anion interactions. For simplicity, direct interactions between the Fe atoms and the electronegative groups of the acceptors are omitted in the upper part of the figure.

Investigation into the local structures of both complexes again indicated that the origin for the valence localization is ascribable to electrostatic stabilization. Both of these crystals contain the same types of centrosymmetric dimer units of the donors, in which Cp rings and alkyl groups have van der Waals contacts near the unit center. Figure 13 shows an illustration of the dimer units together with the arrangement of neighboring molecules. Interestingly, locations of the cationic centers are opposite in both complexes: in **2a**, the formal charges are located on the inner Fc sites, whereas in **2b**, they are on the outer Fc sites. In complex **2a**, Fe(2) interacts more strongly with the anions than Fc(1), which stabilizes the charge localization on Fc(2). The Fc(2) unit interacts with four cyano groups of the acceptors

[−CN···Fe(2) distances: 4.5−5.2 Å], whereas the Fe(1) unit interacts with one CN group [−CN···Fe(2) distances: 4.6 Å] and two sulfur atoms [Fe(2)···S distances: 4.6−4.7 Å] of the acceptors. In addition, the outer Cp ring of the former unit contacts with the alkyl group of the adjacent donor, whereas that of the latter unit contacts with the ferrocenium unit of the adjacent cation [Cp(centroid)···Fe(2) distance: 4.9 Å; Figure 12]. In this arrangement, charge localization on Fc(2) becomes again favorable to avoid cation−cation interactions. In complex **2b**, several close distances were found between the ferrocenium unit involving Fe(2) and the anions, which strongly stabilizes charge localization on Fc(2). The Fc(2) unit interacts with three cyano groups of the acceptors [−CN···Fe(2) distances: 4.2−4.6 Å], whereas the Fe(1) unit interacts with two CN groups [−CN···Fe(1) distances: 4.8−5.0 Å]. More importantly, the outer Cp ring of the Fc(2) unit has a strong face-to-face interaction with one of the central five-membered rings of the anion (centroid−centroid distance: 4.07 Å; Figure 13), whereas the Fc(1) unit only contacts with the alkyl group of the adjacent donor. Therefore, the electrostatic interactions that probably bring about charge localization are stronger in **2b** than in **2a**, which reasonably accounts for the valence-ordering tendency observed in Mössbauer spectra.

Magnetic Susceptibilities. Magnetic susceptibilities of complexes **1a**, **2a**, and **2b** are shown in Figure 7 in the form of χT vs T plots. The magnetic behavior in **1a** was briefly described in a previous section. The χT values of **1a** and **2a** decrease monotonically with decreasing temperature, whereas that of **2b** is nearly temperature-independent. These magnetic susceptibilities are dominated by the contribution of the donor spins, with the χT values (0.5−0.7 emu K mol^{-1}) being reasonable for biferrocenium cations.[46] The spin−Peierls transition in **1a** appears as a slight decrease of χT at around 130 K, but **2a** exhibits no sign of magnetic transitions despite having a magnitude of overlap integrals between the acceptors similar to that in **1a**. Consistently, phase transitions were not found in **2a** by calorimetric measurements. In complex **2b**, because the $[Co(mnt)_2]_2$ unit is diamagnetic, the magnetic susceptibility contains only the contribution of the donor spins. Therefore, the temperature dependence for **2b** was analyzed by applying a modified Curie−Weiss law, $\chi = C/(T - \theta) + q$, where q is a term for temperature-independent paramagnetism.[20] The parameters of best fit were $C = 0.628$ emu K mol^{-1}, $\theta = -0.23$ K, and $q = 1.64 \times 10^{-4}$ emu mol^{-1}. The acceptor columns in **1a** and **2a** can be regarded as $S = {}^1/_2$ Heisenberg chains, in which strong antiferromagnetic interactions prevail, considering the large overlap integrals between the acceptors. The decreasing temperature dependence of magnetic susceptibilities in these complexes results mainly from the contribution of the acceptors, but depopulation of the spin−orbit states of biferrocenium cations seems to have a marked contribution.[47] The data were analyzed in terms of the sum of the modified Curie−Weiss law and a Bonner−Fisher model to estimate magnetic interactions in these compounds;[48] the analytical expression for the latter is found in the literature.[49] For simplicity, we assumed a uniform Heisenberg model because the overlap integrals were comparable and θ was fixed at 0 K. For compound **2a**, the parameters of best fit were $C = 0.486$ emu K mol^{-1} and $J/k_B = -173.1$ K. In those calculations, we assumed the same q values as those for **2b**; the g value for $Ni(mnt)_2$ anions was fixed at 2.043.[14] We should note that these analyses are tentative: the analyses are simplified, and error estimations of J are unavoidable, mainly because of the large background by the ferrocenium spins and of the alignment effect originating from anisotropy of the g-factor values of the ferrocenium spins.[50] In particular, the q values for **1a** and **2a**, and consequently the actual values of J, may be somewhat larger than these values. Nevertheless, the present analyses afford a rough estimate of the consistency of magnetic interactions with molecular arrangements.

Conclusions

We prepared $M(mnt)_2$ salts of 1′,1‴-diisopropyl- and 1′,1‴-diisopropyl-1,1″-biferrocene and investigated their structures and valence states. All complexes were of the 1:1 (or 2:2) D/A mixed-valence biferrocenium salts. It is noteworthy that a spin−Peierls transition was found at 133.2 K in the $Ni(mnt)_2$ complex **1a**. The transition temperature is exceptionally higher than those in other organic systems. Furthermore, a two-step valence transition was observed in **1a**. This novel phenomenon was found to originate from the presence of two crystallographically independent cations that have different valence-ordering temperatures. The valence orderings of the biferrocenes are the thermal depopulation processes resulting from the asymmetrical environment around the cation. The valence ordering at lower temperature is coupled with spin−Peierls dimerization of the acceptors, which causes asymmetry of the crystal environment. For this reason, the two-step transition can be regarded as a consequence of introducing the open-shell $Ni(mnt)_2$ anion.

As to the origin of the valence ordering in biferrocenium salts with inorganic anions, there are discussions on factors such as the packing effect, zero-point energy differences, intermolecular interactions, etc.[1−5] However, the mechanism in the complexes with $M(mnt)_2$ turned out to be simple; investigation of local donor−acceptor arrangements in the crystals demonstrated that the cause of the valence ordering can be understood in terms of local electrostatic interactions; in all of the cations, charge localization was found to occur such that cation−anion interactions stabilize the valence ordering.

Acknowledgment. This work was supported financially and by a Grant-in-Aid for Scientific Research in Priority

(46) (a) Morrison, W. H., Jr.; Krogsrud, S.; Hendrickson, D. N. *Inorg. Chem.* **1973**, *12*, 1998. (b) Cowan, D. O.; Candela, G. A.; Kaufman, F. *J. Am. Chem. Soc.* **1971**, *93*, 3889.

(47) (a) Hendrickson, D. N.; Shon, Y. S.; Gray, H. B. *Inorg. Chem.* **1971**, *10*, 1559. (b) Figgis, B. N.; Gerloch, M.; Mason, R. *Proc. R. Soc. London, Ser. A* **1969**, *309*, 91.

(48) Bonner, J. C.; Fisher, M. E. *Phys. Rev.* **1964**, *135*, A640.

(49) Hatfield, W. E.; Weller, R. R.; Hall, J. W. *Inorg. Chem.* **1980**, *19*, 3825.

(50) Miller, J. S.; Glatzhofer, D. T.; Vazquez, C.; McLean, R. S.; Calabrese, J. C.; Marshall, W. J.; Raebiger, J. W. *Inorg. Chem.* **2001**, *40*, 2058.

Areas (No. 16038224, Novel functions of molecular conductors under extreme conditions) from Japan's Ministry of Education, Culture, Sports, Science and Technology. We thank Dr. Mikio Ueda for analysis of the magnetic data, Shinya Suzuki for the preparation of **1a**, and Dr. Ryo Horikoshi (Toho University) for elemental analysis. We also thank Dr. Michio M. Matsushita and Prof. Tadashi Sugawara (The University of Tokyo) for their help with the low-temperature structure determination of **1a**. We are grateful also to Masaru Nakama (WarpStream Ltd., Tokyo, Japan) for providing Web-DB computer systems. We thank PRESTO, JST (Japan Science and Technology Corp.), for the loan of experimental equipment. This work was performed using facilities of the Institute for Solid State Physics, The University of Tokyo.

Supporting Information Available: Tables of detailed crystallographic data, atomic positional parameters, anisotropic displacement parameters, and bond length and angles in CIF format. This material is available free of charge via the Internet at http://pubs.acs.org.

IC048285U